



Ballistic performance of Cross-laminated Timber (CLT)

K. Sanborn^a, T.R. Gentry^a, Z. Koch^b, A. Valkenburg^b, C. Conley^b, L.K. Stewart^{*,a}

^a Department of Civil and Environmental Engineering, Georgia Institute of Technology, Atlanta, Georgia, USA

^b United States Military Academy, West Point, NY, USA



ARTICLE INFO

Keywords:

Ballistics

CLT

Cross-laminated Timber

Southern pine

Spruce pine fir

ABSTRACT

Cross-laminated Timber (CLT) is a relatively new building material that has gained recent attention in the United States construction industry. CLT is a prefabricated, engineered wood product, composed of three or more plies of lumber with alternating ply directions. CLT is relatively strong and stiff, with the potential to meet the requirements for structures that are subjected to a variety of loading conditions. While CLT's response to static, dynamic (i.e., seismic), and fire loads has been characterized in the past, its response to the loads seen in force protection scenarios (i.e., blast or ballistic) is much less understood.

In order to begin to fill this gap in knowledge, one of the first known sets of ballistic experiments were conducted on CLT and the results were used to develop and validate predictive models. This article describes the results of 122 ballistic experiments conducted at the United States Army Engineer Research and Development Center (ERDC). The experiments were conducted on two species of CLT of varying thicknesses: Spruce Pine Fir-South and Southern Yellow Pine. The experiments measured either penetration depth or residual velocity over a range of intermediate striking velocities. The effects of weathering (i.e., moisture content) were also explored on a data set.

The results of the experiments were compared to existing United States Unified Facilities Criteria models for predicting the ballistic response of wood. The findings show the deficiencies in utilizing this wood model for CLT and explore alternate models for prediction. In general, it was found that models that incorporate both projectile and CLT target parameters most accurately predict the response. Most importantly, the results reinforce the necessity for re-calibration of models as new parameters are added to the CLT ballistic characterization database.

1. Introduction

1.1. Background

Cross-laminated Timber (CLT) is an engineered wood product that is a relatively new structural building material for use in place of, or in conjunction with, concrete, masonry and steel. While builders and designers have used engineered wood products such as plywood and glue-laminated (glulam) products for over a century, CLT is a relative newcomer to the market and falls in the category of mass timber [1]. The first patent for CLT was issued in 1985 in France and was introduced widely in the 1990s in Austria and Germany. Through the use of this construction material in these countries, the material system has gained momentum, with international building codes adopting its use for construction [2,3]. In the last decade, global interest in CLT expanded into North America, especially in the densely forested areas of Canada and the Pacific Northwest region of the United States. The interest was largely motivated by the inherent advantages of wood as a renewable resource.

1.2. Cross laminated Timber (CLT)

Wood's strength is dependent on the grain direction. Specifically, wood has independent properties along three axes: longitudinal, radial, and tangential. These axes and their orientation with respect to the grain direction on a small element are shown in Fig. 1(a) [4,5]. Important wood properties with respect to each of the axes include tensile, compression, and shear properties. These properties depend on orientation: parallel or perpendicular to the grain. Radial and tangential axes are both perpendicular to the grain and longitudinal is parallel to the grain. It is difficult to assess the radial and tangential properties of wood and many failure modes occur with a mixture of radial and transverse mechanisms. Therefore, in wood design, the radial and tangential properties are combined into "transverse" properties and the overall wood member is considered transversely isotropic.

CLT is a strategically manufactured system that optimizes the properties from each direction by combining wood in a layered composite. A CLT panel is formed by stacking solid sawn lumber boards, as shown in schematic form in Fig. 1(b). The layers are secured together

* Corresponding author.

E-mail address: lauren.stewart@ce.gatech.edu (L.K. Stewart).

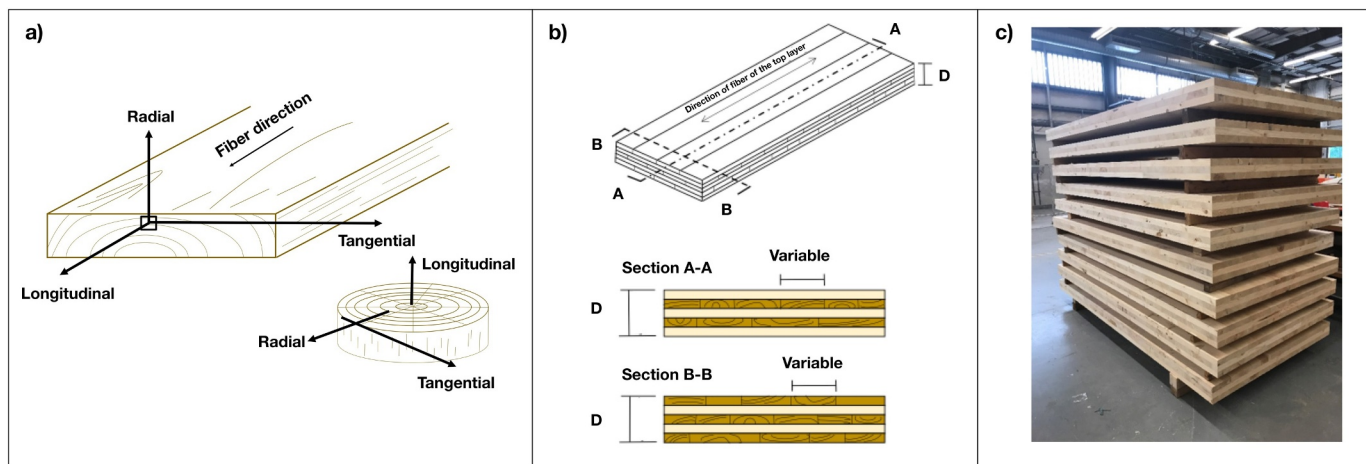


Fig. 1. a) Wood axes with respect to grain direction, b) Cross-Laminated Timber panel schematic, and c) Three-ply Cross-Laminated Timber panels.

with polyurethane, melamine, or phenolic-based adhesive. Panels typically consist of an odd number of layers, varying from three to nine. Three-ply CLT panels are shown in Fig. 1(c). Similar to a sandwich panel, the outer layers and alternating layers of the inner core are oriented such that the primary strength axis of the wood corresponds to the direction of primary loading.

The thickness of each layer in the CLT varies from 0.625 to 2 in. (16 mm–51 mm). The width of the individual layers varies from approximately 2.4 to 9.5 in. (60 mm–240 mm) [3]. The full panel size varies by manufacturer and specific customer need, with typical widths of 2 feet (0.6 m), 4 feet (1.2 m), 8 feet (2.4 m), and 10 feet (3 m) and lengths that can reach upwards of 60 feet (18 m). Last, the thickness of the entire panel with all its layers can be up to 20 in. (508 mm) for panels manufactured under the current standard rating guidance from the Engineered Wood Association (APA) [6].

1.3. CLT classification

In the United States, CLT is classified by graded. Table 1 lists the wood types and rating for the most common CLT grades. The “E” designation refers to timber based on mechanically rated or machine stress rated (MSR). The “V” designation refers to visually graded timbers. Each grade of CLT is composed of specific grades of specific species in the parallel and perpendicular layers. Some CLT grades use a combination of E-rated and V-rated timbers in different layers.

1.4. Mechanical properties

In general, the mechanical properties for CLT are evaluated through two methods: 1) Using the known properties of individual boards/layers and the laminated plate theory to establish overall properties; or 2) The determination of properties based on the full-section testing of CLT elements [7]. Key mechanical properties required for design

include modulus of rupture, compression and tensile strength parallel to grain (longitudinal properties), compressive and tensile strength perpendicular to grain (transverse properties), in-plane shear strength, rolling shear strength, and hardness. Because wood is a cellular solid, mechanical properties vary as a function of density and moisture content, and so these must be measured when completing mechanical tests of wood. A given CLT panel is made of tens of individual boards, each having its own set of properties. Consequently, it is difficult to predict the exact failure mechanism in a given panel.

The performance of a CLT panel is also dependent on the efficacy of the adhesive bonds between the plies. The initial quality of the bond is established using shear specimens similar to those cut from solid wood, but with the bond line centered in the shearing plane per ASTM D905, Standard Test Method for Strength Properties of Adhesive Bonds in Shear by Compression Loading [8]. The surfaces of the sheared specimen are assessed for adhesive failures (unacceptable), cohesive failures (acceptable) or substrate/wood failures (preferred) according to ASTM D5266, Standard Practice for Estimating the Percentage of Wood Failure in Adhesive Bonded Joints [9].

When considering impact resistance, an important characteristic for wood design is hardness, *H*. Hardness is seen as a measure of durability and structural quality combined in one metric. Commonly, hardness is defined as the resistance to indentation through the modified Janka hardness test, as outlined in ASTM D1037, Standard Test Methods for Evaluating Properties of Wood-Base Fiber and Particle Panel Materials and ASTM D143 Standard Test Methods for Small Clear Specimens of Timber [10–12]. The Janka test measures the force required to embed a 0.444 in (11.3 mm) diameter ball into the wood to one-half of the ball’s diameter. The force values of hardness through the testing are often combined with strength parameters like the modulus of rupture, ultimate compressive stress parallel to the grain, and are proportional to density of the wood. Hardness also varies with moisture content.

As a natural material, wood is subject to significant variation in

Table 1
Wood lamination composition by CLT grade [6].

| Grade | Composition |
|-------|---|
| E1 | Spruce Pine Fir MSR lumber in all parallel layers and No.3 Spruce Pine Fir lumber in all perpendicular layers |
| E2 | Douglas fir-Larch MSR lumber in all parallel layers and No. 3 Douglas fir-Larch lumber in all perpendicular layers |
| E3 | Eastern Softwoods, Northern Species, or Western Woods MSR lumber in all parallel layers and No. 3 Eastern Softwood, Northern Species, or Western Woods lumber in all perpendicular layers |
| E4 | Southern pine MSR lumber in all parallel layers and No. 3 Southern pine in all perpendicular layers |
| V1 | No. 2 Douglas fir-Larch lumber in all parallel layers and No. 3 Douglas fir-Larch lumber in all perpendicular layers |
| V2 | No. 1/No. 2 Spruce Pine Fir lumber in all parallel layers and No.3 Spruce-pine-fir in all perpendicular layers |
| V3 | No. 2 Southern pine lumber in all parallel layers and No. 3 Southern pine lumber in all perpendicular layers |
| V4 | SmartLam CLT manufactured with Spruce Pine Fir south lumber in accordance with custom layup combination approved by APA |

mechanical properties. Wood variability can be a product of tree species, growing environment, and tree age. With CLT, which acts as a multi-layer sandwich composite, the variation in the global system behavior is seemingly reduced as the composite nature homogenizes the variability, but the variability should be considered for behaviors that are more localized.

1.5. CLT performance in extreme events

As CLT becomes further adopted into U.S. and global construction, the performance of the structural system must be evaluated and characterized under a variety of loading conditions that are typical in building design. These loading conditions include those associated earthquake and fire.

Experiments have shown that structures built with CLT perform well under seismic loading conditions. CLT wall systems have shown to effectively handle lateral loading conditions, even under extreme earthquake loads [13,14]. The layering of timbers in a CLT panel offers more ductile behavior than some other mass load bearing construction materials such as reinforced concrete; however, when considering CLT for use in seismically active areas, care must be taken in the design of the connections. CLT walls appear to provide structural redundancy and CLT structures are less susceptible to soft story failures than other platform framed systems [3].

Research on the fire resistance of CLT panels has been conducted using full-scale experiments over the last decade [15]. Recently, CLT demonstrated the capability of meeting U.S. fire safety requirements related to flame spread and fire resistance outlined in ASTM E84-15b, Standard Method of Test for Burning Characteristics of Building Materials and ASTM E119-16, Standard Test Methods for Fire Tests of Building Construction and Materials, respectively [16–18].

The characterization of CLT for force protection (i.e., blast and ballistic effects) is much less mature. The first set of explosive blast experiments on three CLT structures were completed by WoodWorks at Tyndall Air Force Base in 2017 [19]. The results of the testing shows promise for properly detailed CLT structures to meet General Services Administration (GSA) performance requirements for blast. To the authors' knowledge, prior to this effort, no experiments had been conducted for assessing the ballistic performance of CLT. Therefore, no tools exist and there is no basis for designing or analyzing CLT structures for ballistic threats. To fill this gap in knowledge, 152 experiments were conducted at the U.S. Army Engineer Research and Development Center (ERDC) in order to develop an understanding.

2. Experiment description

2.1. Test setup

The ballistic experiments were conducted at the U.S. Army Corps of Engineers' Engineer Research and Development Center (ERDC) in the Fragment Simulating Facility. The experimental test setup (Fig. 2) consisted of an indoor, conditioned, ballistic range with a smooth bore powder gun with a 0.50-caliber barrel. Fig. 3(a) shows the firing apparatus. While the firing system can be adapted for multiple barrels, only a 0.50-caliber barrel was used. The firing apparatus was mounted and secured to a table to prevent movement with test shots. Four infrared photoelectric velocity screens were connected to two chronographs in order to capture two different velocity measurements as the projectile moved down range in the direction of the target.

The data from the screens was used to determine the striking velocity, v_s , using Eq. (1), based on the measured velocities and known distances between each of the screens and between the final screen and target. In the equation, v_1 is the velocity as determined by screens one and three (first and third screen the projectile passes), and v_2 is the velocity as determined by screens two and four. L_1 is the distance from which v_1 and v_2 were measured (known from test set-up), and L_2 is the

distance between where v_2 was measured and the impact side of the test specimen (front face of the target).

$$v_s = v_2 + \left(\frac{L_2}{L_1}\right)(v_2 - v_1) \quad (1)$$

The CLT test specimens were mounted to a steel frame using ratchet straps, as shown in Fig. 3(b). The frame also had a small shelf to rest the specimen, which helped ensure it was level and at the same location for each test. The steel frame was clamped with c-clamps to a small hydraulic lift on rails affixed to the facility floor. This lift enabled the repositioning of the target both horizontally and vertically to allow for multiple shots in each test specimen. Each specimen was shot five times, in five locations, equidistant apart. The shot pattern was held constant for each test, with one shot in the center and the four remaining shots near the four corners of the specimen.

Two Phantom high-speed cameras were mounted on tripods to capture the ballistic event from two perspectives. One was focused on the front target face and the second was positioned to capture the back face and behind the target to acquire the residual velocity. The cameras were set on an acoustic trigger and captured the event in 512 x 384 pixel resolution at 14,035 frames per second. An additional set of two infrared photoelectric velocity screens connected to a chronograph were also used at back face of the specimen; however, wood debris occasionally caused a misreading and thus analyzed high-speed video was the primary source for residual velocity data. With the video, the researcher could identify the projectile from the debris and ensure an accurate residual velocity was recorded.

2.2. CLT Ballistic targets

Two different softwood CLT were used as targets: Spruce Pine Fir-South (SPF-S) and Southern Yellow Pine (SYP). The square targets varied in thickness (i.e., number of plies) and were 12 in. by 12 in. (30.5 cm by 30.5 cm) in height and width. These two softwood species were used for testing due to commercial availability and interest in the incorporation of a local forest product, widely available in the state of Georgia and the rest of the southeastern U.S. The SPF-S was manufactured into a V4 grade CLT by the manufacturer SmartLam to the APA standard specifications [6].

Currently, there is no commercial manufacturer that produces CLT made of SYP. Therefore, the SYP specimens were manufactured at the Georgia Institute of Technology's Digital Fabrication Laboratory (DFL). They were made in accordance with the guidelines and standards presented in the CLT Handbook: U.S. Edition and Standard for Performance-Rated Cross-Laminated Timber ANSI/APA PRG 320–2012 (PRG 320) [6]. For selection and grouping, the moisture content was checked with a pin resistance moisture meter and each lamina piece was weighed in order to minimize variation in moisture content and density within layers. Prior to gluing and pressing, 2 in. by 8 in. (5.1 cm by 20.3 cm) lumber was planed to 7 in. (17.8 cm) wide by 1.375 in. (3.5 cm) thick and trimmed to 14 in. (35.6 cm) long to fit the size limitations of the small hydraulic press. These dimensions remained within the recommended maximum lamination thickness to width ratio of 3.5. As recommended, the wood was planed within two hours of adhesive application. This allowed for a reduction in surface oxidation, surface aging, and dimensional instability thus preparing the wood for a more effective bond [3]. The pieces of cut lumber were then set in the desired lay-up with orthogonally oriented layers, as shown in Fig. 4(a). Polyurethane adhesive was applied in thin ribbons parallel to the grain direction and spread evenly across the surface. Each successive layer was stacked as soon as the glue was spread. An average of 29.3 g of adhesive per square foot of lumber was used. The 14 in. by 14 in. (36 cm by 36 cm) specimen block was held in place laterally with two plastic corner braces and ratchet straps as the expanding adhesive caused the pieces to push out and create undesirable gaps between the pieces in a single layer. The braces and straps were not intended to apply a specific clamping pressure but to hold the small pieces in place horizontally. Layers, or plies, were added to reach the

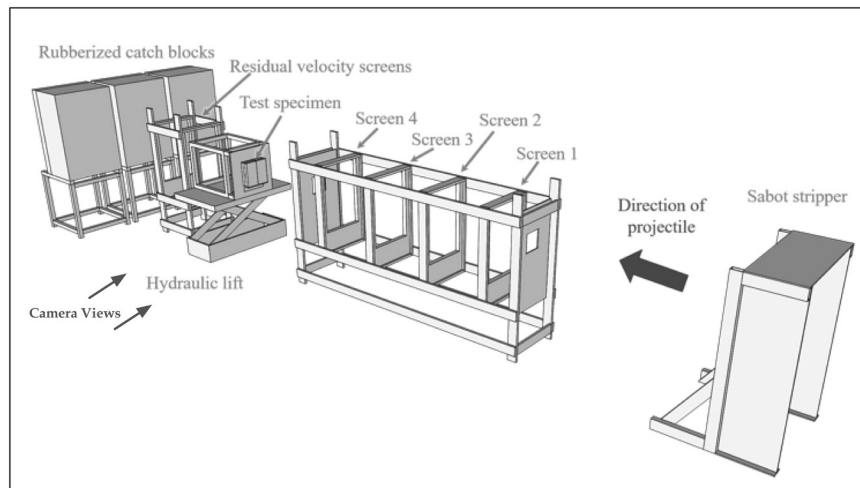


Fig. 2. Ballistic CLT experimental setup at the US Army Engineer Research and Development Center (ERDC).

desired number and then the specimen was pressed using a small hydraulic press, applying 100 psi (0.7 MPa) clamping pressure for a period of two hours (Fig. 4(b)). After removal from the press, the excess adhesive was cleaned off the edges and the specimen were trimmed to a standard 12 in. by 12 in. (30.5 cm by 30.5 cm) size.

The two species have different mechanical properties. Table 2 gives a summary of the property for each wood species as well as the experimental method or procedure that was used. The SYP test specimens were not large enough for significant static strength and stiffness testing in bending but based on the lumber used for construction, would be expected to perform as well as the V3 CLT grade specifications in PRG 320 with layups on No. 2 Southern pine lumber in all parallel layers and No. 3 Southern pine in all perpendicular layers, as indicated in Table 1. Additional mechanical properties not tested in this research can be approximated using previous research for the specific type of wood and CLT grade [33–35]. It should be noted that any property relating to bulk modulus should use the sub-sonic relations.

2.3. Projectiles

The projectile for the testing was a small caliber, 0.5 in. (12.7 mm) steel sphere constructed of hardened impact-resistant S-2 tool steel. This projectile, with striking velocities of 500 to just over 3500 ft/s (180 - 1200 m/s), was selected as a benchmark for CLT due to the vast ERDC database for ballistic tests using this projectile with other target materials. Additionally, use of the sphere eliminated any security concerns with collecting data as the spheres are purely used in laboratory testing and not a munition for military use in the field. As such, the data presented in this paper is solely from the steel sphere projectiles, although additional data was collected including that from 0.50-caliber Fragment Simulating Projectiles (FSP) [20].

The projectiles were mounted in a 0.50-caliber cartridge with a plastic sabot. The sabot holds the projectile in the cartridge without letting air or moisture into the cartridge interior where the powder burns and initiates the ballistic event. The sabot falls away from the projectile as it moves down range due to a pre-cut perforation and is removed from the experiment by a sabot-stripper in the setup, which is shown in Fig. 2. This device blocks the plastic sabot pieces from continuing in the direction of the velocity screens and the target. The projectile velocity is varied by adjusting the weight of powder in the cartridge.

3. Experimental results

3.1. Test matrix

The ballistic data is grouped based on the outcome of the shot: perforation (full penetration) or partial penetration. If the projectile perforated the CLT specimen, then a residual velocity, v_r , was recorded based on the high-speed video capturing the round exiting the back face of the specimen. If the shot was a partial penetration and thus the projectile remained embedded in the specimen, then the penetration depth, d , was recorded. The breakdown of number of shots by species type and outcome type is shown in Table 3.

3.2. Partial (embedded) penetration experiments

Fig. 5 shows examples of dissected test specimen post test in which the 0.5 in. (12.7 mm) sphere projectile has embedded in the CLT (a) and has perforated the CLT (b). From post test dissections, embedded rounds show the displacement of fractured wood as the projectile passes, as shown in Fig. 5. The damage zone is localized, extending no

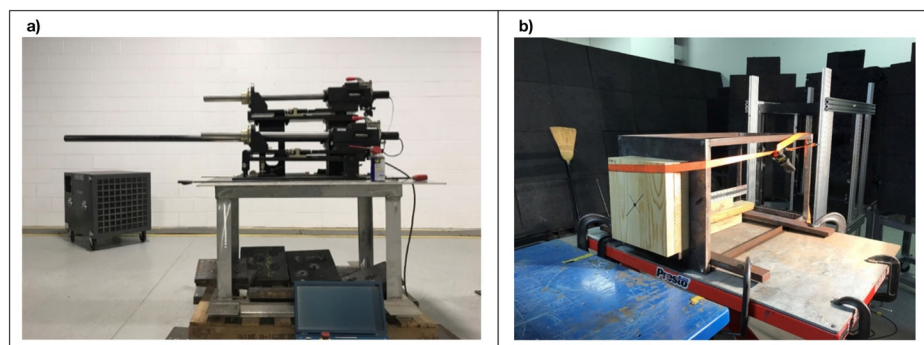


Fig. 3. a) Firing apparatus and b) CLT target specimen (right).

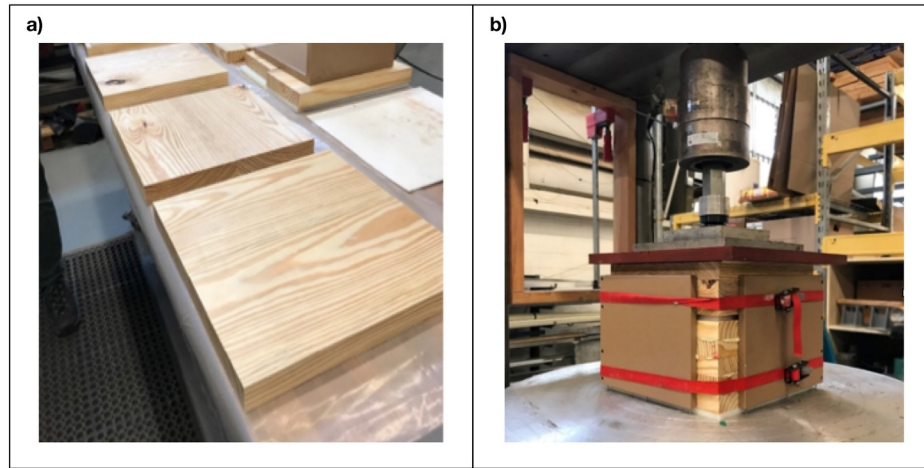


Fig. 4. Southern yellow pine CLT construction: a) Orthogonally oriented plies preparation and b) Plies being pressed at 100 psi (0.7 MPa) in hydraulic press.

more than approximately one-half the sphere’s diameter on each side of the sphere’s boundary. Localized bending in the growth rings is also visible in multiple plies. The fractured wood and some debris was also observed in the cavity created by the projectile. Additionally, splintered sections of the previously penetrated ply are often found in the subsequent ply. Additional information from the dissected sections is given in Sanborn, 2018 [20]. Fig. 6 gives the 0.5 in. (12.7 mm) sphere experimental data for each wood type (SYP or SPF-S) for the 63 cases in which the projectile remained embedded in the specimen. The figure plots the striking velocity, v_s , measured from the velocity screens, in terms of penetration depth, d . The data from the individual experiments is given in Sanborn, 2018 [20].

3.3. Complete penetration (perforation) experiments

Fifty-nine 0.5 in. (12.7 mm) sphere projectile experiments were conducted that resulted in complete penetrations and, therefore, had a corresponding residual velocity. Fig. 5(b) shows an example specimen post test in which the 0.5 in. (12.7 mm) sphere projectile has perforated all the layers of CLT. The exit hole of the projectile in this 3-ply specimen, noted with the white box, appears to be larger than the projectile path. This mechanism is potentially due to scabbing, where a conical section of the back face of the specimen fractures off as debris. Additional information from the dissected sections is given in Sanborn, 2018 [20].

The majority of these tests fell within a smaller band of striking velocities (target velocity was 2,500 ft/s (762 m/s)), as shown in Figs. 7 and 8. Ballistics testing is inherently variable as even factory-produced munitions with the same projectile and powder load shoot at a range of velocities. The goal of these experiments was to conduct multiple shots

Table 2
SPF-S and SYP physical and mechanical properties.

| Property | Method | SPF-S | | | SYP | | |
|--|----------------------|--------------|---------------------------|-----|-------------|------------|-----|
| | | Mean | COV | N | Mean | COV | N |
| Density ⁽¹⁾ , lb/ft ³ (kg/m ³) | | | 28.4 ⁽³⁾ (455) | | | 34.2 (548) | |
| Moisture Content ⁽²⁾ , % | pin meter | | 10.5% | | | 9.0% | |
| Shear Strength Parallel to Grain, psi (MPa) | ASTM D143 Section 14 | 1,300 (8.96) | 27% | 14 | 1600 (11.0) | 13% | 19 |
| Hardness Perpendicular to Grain, lb (N) | ASTM D1037 | 605 (2,690) | 29% | 208 | 656 (2,920) | 30% | 191 |
| Bond Line Shear Strength, psi (MPa) | ASTM D905 | 399 (2.75) | 32% | 5 | 880 (6.07) | 19% | 7 |

(1) Density measured as the average of the entire set of CLT specimens of a given wood species, based on the weights of the 12 in. by 12 in. (30.5 cm by 30.5 cm) shot blocks. (2) Moisture content measured during shear-block testing and CLT production; N greater than 100. (3) Mechanical properties reported to three significant figures.

Table 3
Breakdown of number of ballistic tests by species and outcome type.

| Species | 0.5 in. sphere | | Total |
|----------------------------|----------------|-------------|------------|
| | Embedded | Perforation | |
| Spruce Pin Fir-South | 35 | 20 | 55 |
| Southern Yellow Pine | 28 | 39 | 66 |
| SPF-S and SYP Total | 63 | 59 | 122 |

at multiple specimens at the same approximate striking velocity for comparison between wood species and number of plies.

The data presented in Fig. 7 consists of all 5-ply SPF-S and SYP specimen. In general, as the striking velocity increased, the residual velocity also increased for both species, as expected. The SYP CLT provided more resistance to the projectile than the SPF-S CLT, resulting in smaller residual velocities. The data presented in Fig. 8 consists of both 3-ply and 5-ply SYP specimens. As expected, the residual velocity increased as the striking velocity increased and the residual velocity increased from 3-ply to 5-ply because there was less material to resist the projectile.

4. Effects of weathering on ballistic performance

For certain construction types, the CLT panels could potentially be exposed to the environment. Therefore, a limited number of experiments were conducted to determine the effect of short-term weathering (i.e., moisture content) on the ballistic resistance. Elevated moisture contents of the specimens represented panels that are exposed to rain, snow, and elevated humidity.

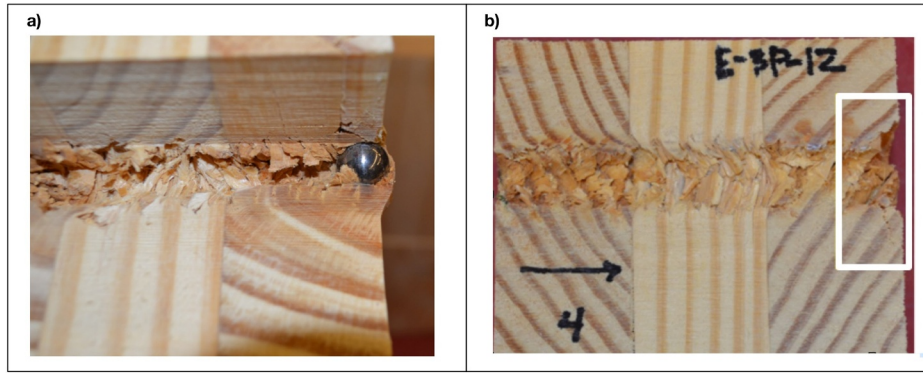


Fig. 5. Post test CLT specimen with a) 0.5 in. sphere embedded and b) perforated.

A 5-ply test specimen of each CLT species was placed in a fog room for three days and a second 5-ply test specimen was submerged in a bucket of water for thirteen days. The purpose of these treatments was to elevate the moisture content of the specimens. The original moisture contents of the four specimen prior to the weathering treatments were in the range of 9 to 11 percent. The fog room was 70 F (21.1 C) and 100 percent humidity. Since there was no mechanism to measure the interior moisture content within the specimens, the weights of the blocks were measured periodically and the increase in density required to achieve the desired moisture content in the test specimens was calculated. When the test specimens were removed from the fog room and water bath, they were weighed and a moisture content reading was taken with a pin-type moisture meter on the exterior surface at each ply. All four test specimens were then subjected to the 0.5 in. (12.7 mm) sphere projectile at an average striking velocity of 2,500 ft/s (762 m/s). Post test, the blocks were cut open to the center shot and an interior moisture content was measured at each ply. Table 4 shows the average exterior and interior moisture contents for both wood species.

The results from the 5-ply dry and weathered specimen are shown in Fig. 9 for the SPF-S and SYP species, respectively. While this represents a relatively small and limited data set, the results suggest that there is no statically significant difference between the moisture content and the ballistic performance within the range of values and parameters explored.

5. Penetration depth models

5.1. Unified Facilities Criteria (UFC) model

Current design guidance for United State Department of Defense (DOD) planning and design of ballistic penetration is detailed in Unified

Facilities Criteria (UFC) 4-023-07, Design to Resist Direct Fire Weapons Effects [21]. This standard provides guidance for facility design with the intent of protection from direct fire weapon effects, which includes small arms ballistic weapons such as pistols, rifles, shotguns and submachine guns up to 0.50-caliber (12.7 mm). The UFC uses the Underwriters Laboratories (UL) ballistic standards for testing and characterizing building elements or assemblies resistance to ballistic effects [22]. The UFC provides an equation for the thickness of wood necessary to resist perforation (see Eq. (2)), referred to as the "UFC equation" for the remainder of this article. In the empirical equation, T_w is the thickness of wood required to prevent perforation (in), v is the projectile impact velocity (ft/s), w is the projectile weight (lb), D is the projectile diameter (in), ρ is the wood density (lb/ft³), and H is the wood hardness (lb).

$$T_w = 9, 837 \left(\frac{v^{0.4113} w^{1.4897}}{\rho \left(\frac{\pi D^2}{4} \right)^{1.3596} H^{0.5414}} \right) \quad (2)$$

The results from using the equation were compared to the CLT ballistic test experiments for the 0.5 in. (12.7 mm) sphere projectile data. This comparison is shown in Fig. 10. While it was expected that this UFC model for perforation thickness would overpredict the response of the penetration depth due to the back face of the CLT having less resistance, this level of overprediction was not acceptable. It is important to note that empirical models developed from ballistic studies can often predict response accurately within some specified range, but that those models should often not be extrapolated for use in conditions other than those from the test scenario used to develop the model without re-calibration. The stark difference between the UFC equation and the CLT data is a perfect example of this. Evidence

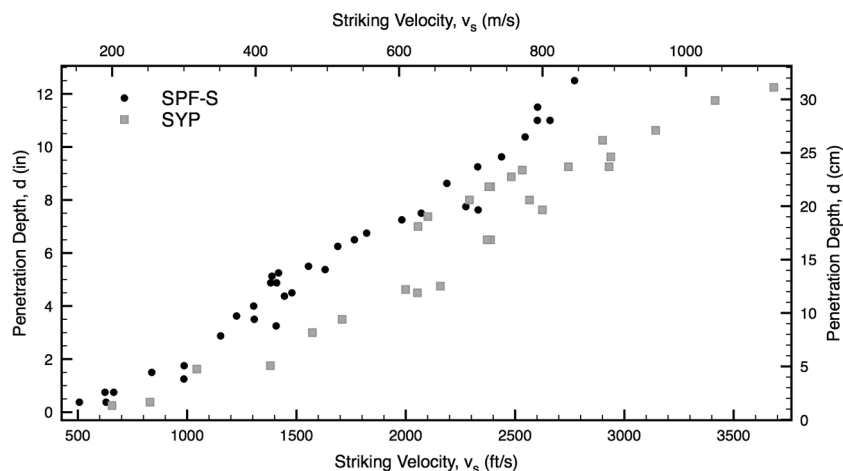


Fig. 6. Impact velocity versus penetration depth data from CLT ballistic experiments for Spruce Pine Fir-South CLT and Southern Yellow Pine CLT targets.

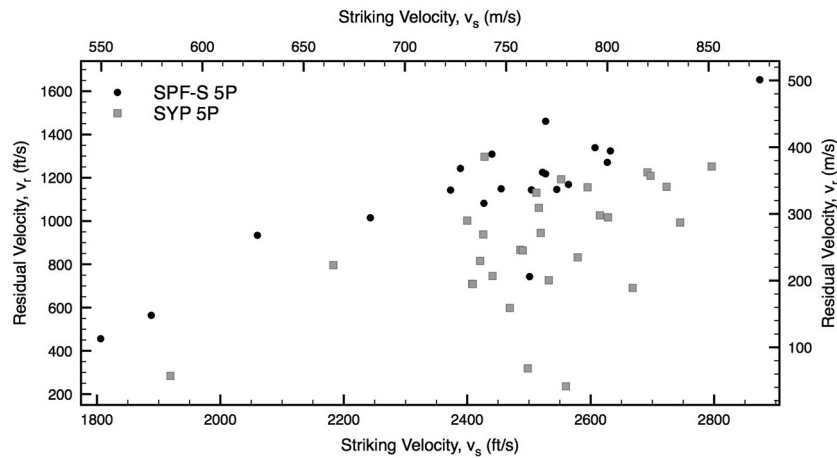


Fig. 7. Striking velocity versus residual velocity data from CLT ballistic experiments for 5-ply Spruce Pine Fir-South and Southern Yellow Pine CLT.

supports that the UFC equation was calibrated based on data taken from the THOR experiments conducted in the 1950’s, and that the experiments used to calibrate the existing equation were completed on relatively thin blocks of wood.

5.2. Classical penetration models

Leonard Euler and Benjamin Robins studied the behavior of the penetration of steel cannonballs in soils with various striking velocities [23]. Shortly after their experiments, Jean-Victor Poncelet began extensive work in the area and proposed an equation, a version of which is shown in Eq. (3) [24]. Today, the equation is known as the Poncelet equation.

$$\frac{d}{dt}(mv) = -A_{cs}c_0 - A_{cs}c_1v^2 \tag{3}$$

Poncelet’s equation states that the instantaneous time rate of change, d/dt , of a projectile’s momentum, mv , is equal to the sum of two retarding forces: 1) a general form of drag that is proportional to the cross-sectional area of the penetrator, A_{cs} ; and 2) a dynamic drag term proportional to the cross-sectional area of the penetrator multiplied by the square of the penetrator velocity, v , a kinetic energy term. The constants, represented by c_0 and c_1 , are dependent on the target material being penetrated. The Poncelet equation describes rigid body penetration and assumes that the cross-sectional area of the penetrator remained constant with no significant mass loss during the projectile’s movement through the target. This assumption is not always accurate as penetrators may experience expansion, mushrooming, fragmentation, and erosion during an impact event [25].

Table 4

Dry and weathered CLT specimens exterior and interior moisture contents.

| Species | Treatment | Average exterior moisture content | Average interior moisture content |
|---------|-----------|-----------------------------------|-----------------------------------|
| SPF-S | Dry | 10.5% | 10.5% |
| SYP | Dry | 9% | 9% |
| SPF-S | Fog Room | 32% | 13% |
| SYP | Fog Room | 28% | 15% |
| SPF-S | Submerged | 38% | 22% |
| SYP | Submerged | 38% | 33% |

Poncelet effectively took the ballistic impact phenomena of a rigid penetrator, known to be governed by the deceleration of the penetrator, and applied mathematics to transform the equation such that a solution could be obtained from measurable data. Because an accurate measurement of deceleration during penetration is difficult to capture with most materials, penetrator depth measurements from experiments across a range of velocities were used to determine material dependent constants in the empirical relationship.

Poncelet assumed that the penetrator is rigid with an unchanging mass. The penetration depth of a projectile thus was recognized to be solely dependent on the deceleration of the projectile in the target and the velocity of the projectile, as shown in Eq. (4), where d represents the final penetration depth, v is the velocity, v_s is the striking velocity, and a is the deceleration.

$$d = \int_{v_s}^0 \frac{v}{a(v)} dv \tag{4}$$

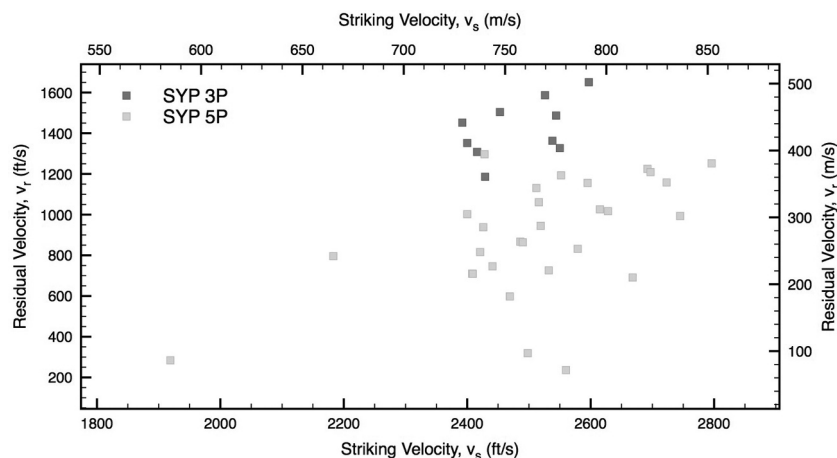


Fig. 8. Striking velocity versus residual velocity data from CLT ballistic experiments for 3-ply and 5-ply Southern Yellow Pine CLT.

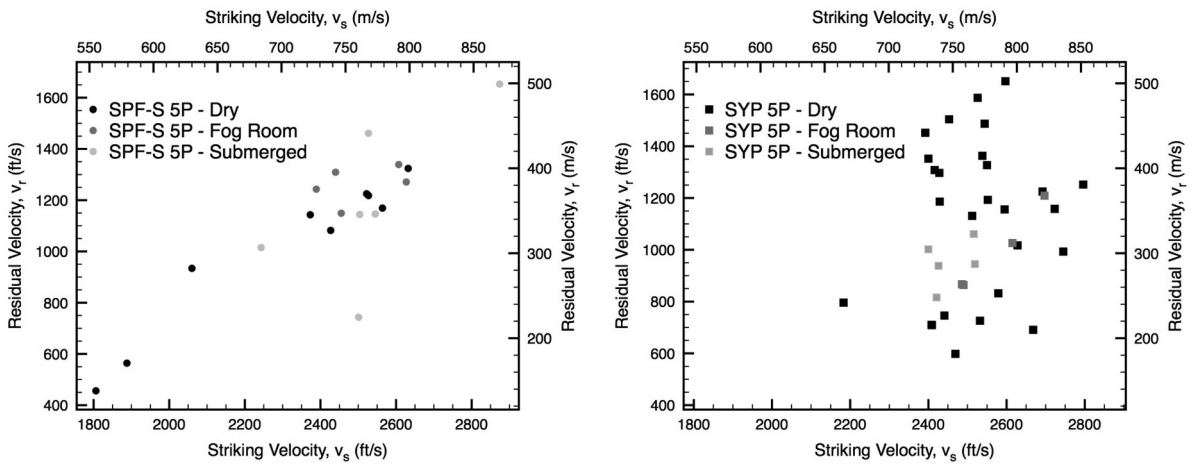


Fig. 9. Striking velocity versus residual velocity data from SPF-S CLT (left) and SYP CLT (right) ballistic experiments for weathered specimen (i.e., varying moisture content).

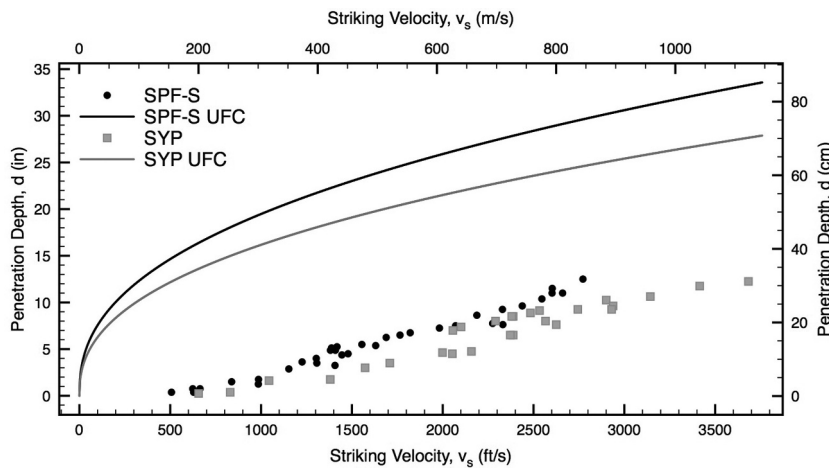


Fig. 10. Impact velocity versus residual velocity data from CLT ballistic experiments for Spruce Pine Fir-South and Southern Yellow Pine CLT targets compared with prediction model of UFC 4-023-07.

Table 5
Classic penetration equations and associated penetration depth expressions.

| Model | Deceleration | Penetration depth | Calibrated constants |
|--------------|---------------------------|--|---------------------------|
| Euler–Robins | $a = C = \text{constant}$ | $d = \frac{v_s^2}{2C}$ | $C = 3.776e5$ |
| Poncelet | $a = C + Bv^2$ | $d = \frac{1}{2B} \ln \left(1 + \frac{Bv_s^2}{C} \right)$ | $C = 1.887e5, B = 0.0672$ |
| Resal | $Av + Bv^2$ | $d = \frac{1}{B} \ln \left(1 + \frac{Bv_s}{A} \right)$ | $A = -0.0497, B = 363.9$ |

Early in the investigation of penetration mechanics, various theories were proposed to describe the relation between deceleration and velocity. Most were based on a general expression for the deceleration term shown in Eq. (5), where v represents velocity, $a(v)$ is deceleration relative to velocity and $A, B,$ and C are constants that must be determined empirically. The terms on the right side of the equation are commonly associated with the cohesive resistance of the target, $C,$ a frictional effect, $Av,$ and acceleration of target material in the impact area, $Bv^2.$

$$a(v) = C + Av + Bv^2 \tag{5}$$

Classic penetration equations based on these fundamental relationships and assumptions were developed by Euler and Robins [26,27], Poncelet [28], and Resal [29]. Through integration, the expression for deceleration relative to velocity can be transformed into an

expression for the final penetration depth, $d,$ in terms of striking velocity, $v_s.$ Table 5 gives the penetration ballistics equations credited to each scientist as well as the calibrated constants that were derived by the authors for this dataset.

The results from the ballistic test series and the Levenberg-Marquardt algorithm [30] were used to determine the constants in the three classical penetration models. The calibrated constants are given in Table 5. These models have also been used by other researchers for solid wood [31]. The results of the three models are shown in Fig. 11 for both species of CLT data combined. The errors from the models and comparisons are discussed in Section 6.6. It should be noted that the reference values [3] for hardness and density were used in this calibration because it is expected that a typical user would not necessarily conduct material testing. The measured values are provided above in Table 2 as well as in the spreadsheet provided in the linked document. The models can be re-calibrated using the same procedure and the measured properties, if desired.

5.3. Force law model

Based on the classical equations with variations of the deceleration equation, an additional physics-based model was developed and calibrated to the CLT data. This model was based on the concept of a resisting force of the target specimen reducing the velocity of the projectile. This resisting force acts as an external force on the projectile,

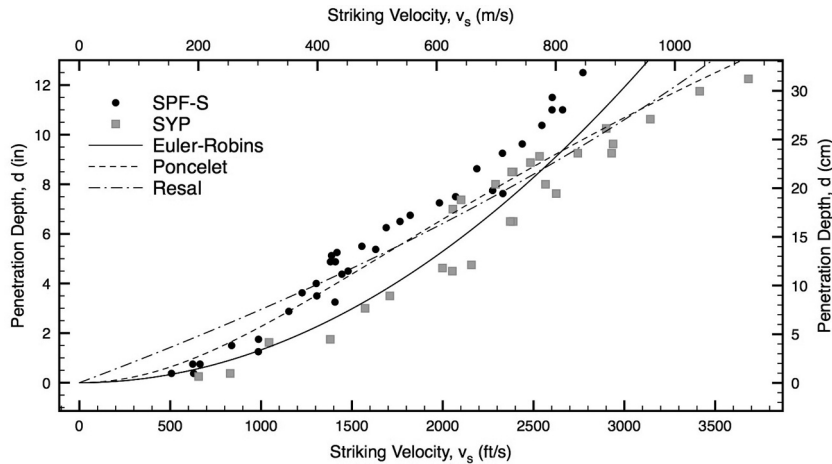


Fig. 11. Euler–Robins, Poncelet, and Resal penetration depth models calibrated with CLT data.

compelling it to reduce its velocity or even stop completely. The resisting force is included as a general quadratic form and the residual velocity, v_r , can be calculated as shown in Eq. (6). In the equation, v_s , is the striking velocity, x is the distance traveled in the target, and a , b , and c are model constants.

$$v_r = v_s - ax^2 - bx - c \tag{6}$$

When the CLT specimen stopped the projectile and the residual velocity was zero the equation can be rewritten and solved for the distance, x , as shown in Eq. (7). If the depth of penetration is considered x is the distance traveled in the target, T_w .

$$x = d = \frac{1}{2a}(\sqrt{b^2 + 4v_s a - 4ac} - b) \tag{7}$$

Eq. (7) was calibrated to the CLT ballistic data, creating an empirical, physics-based model. Using the Levenberg–Marquardt method, the parameters were found for the Force Law model. This model considered no material factors for the target or the projectile other than striking velocity. Fig. 12 shows the curve of the model fit to both species of data combined. The calibration constants for each of the is given in Table 6. The errors from the models are discussed in Section 6.6.

5.4. THOR models

An example of a purely empirical approach is the equation given in the THOR reports [32]. In the 1960s the Ballistic Analysis Laboratory and Ballistic Research Laboratory studied penetration for metallic and non-metallic materials and published reports with empirical equations developed from testing. The projectiles used in the THOR research were steel fragments and experimental data was characterized by fragment size, striking velocity, and the angle of obliquities. A base equation was developed with five experimental variables and five adjustable constants. This equation, for calculating residual velocity, is shown in Eq. (8). In the equation, v_r represents fragment residual velocity, v_s is the fragment striking velocity, t is the target thickness, A is the average impact area of fragment, θ is the angle of obliquity, w is the weight of the original fragment, m_r is weight of residual fragment, and c , α , β , γ and λ are calibration constants.

$$v_r = v_s - 10^c(tA)^2 w^\beta (\sec\theta)^\gamma v_s^\lambda \tag{8}$$

The general THOR equation shown above can be rewritten for conditions when the residual velocity is zero as there is no perforation. The scope of this research is limited to normal impacts, an angle of obliquity of zero, which simplifies the formula and allows for exclusion of the variable, θ , and its associated parameter, γ . Next, the equation can be rearranged to solve for the thickness at which the residual velocity is zero, as shown in Eq. (9), where the constants are renamed to l ,

m , and n . Finally, assuming that the relation holds between predicting the perforation thickness, T_w , and the penetration depth, d , the equation can be written in terms of penetration depth as shown in Eq. (10) with different calibration constants f , g , and h .

$$T_w = \frac{1}{A} \left(\frac{v_s^l}{10^m w^n} \right) \tag{9}$$

$$d = \frac{1}{A} \left(\frac{v_s^f}{10^g w^h} \right) \tag{10}$$

Using the same nonlinear least square fitting method as the previous models, the general THOR model was calibrated to the SPF-S CLT and SYP CLT data combined as shown in Fig. 13, with calibration constants given in Table 7. The error from the model is discussed in Section 6.6.

Since the general THOR equation is an empirical formula, it is possible to include additional variables of interest with little difficulty. This led to the development of a new CLT model based on the general THOR equation but with the addition of the target density, ρ , and a strength parameter, wood hardness, H . Since it was observed in previous models and documented in the THOR reports that unchanging variables could effectively be excluded from the curve-fitting model for simplification, the variable for projectile weight, w , was removed. Because the same projectile weight was used in all tests, inclusion in the model simply acts as an additional constant instead of a calibrating parameter.

Eq. (11) gives the CLT THOR-based equation developed for the CLT experiments. The equation includes the striking velocity, v_s , of the projectile but no other projectile variables since the same projectile was used for the entire data set. It also includes the density, ρ , and hardness values, H , of the CLT specimens. The calibration constants are represented as C_1 , a , b , f , and g .

$$d = C_1 \left(\frac{v_s^f}{10^g \rho^a H^b} \right) \tag{11}$$

Because the model is material dependent, two curves are generated from the single calibrated calibrated model: one curve for SPF-S and one curve for SYP. Fig. 13 shows the CLT THOR curves calibrated to both species of CLT data with calibration constants given in Table 7. The errors from the models are discussed in Section 6.6.

5.5. CLT UFC Model

While the UFC model for wood discussed in Section 5.1 did not fit the experimental data of embedment depth well, it did incorporate variables both measurable and relevant to a ballistic penetration event. A generic version of the UFC equation with unsolved calibration constants (C_1 , a , b , c , and d) is shown in Eq. (12).

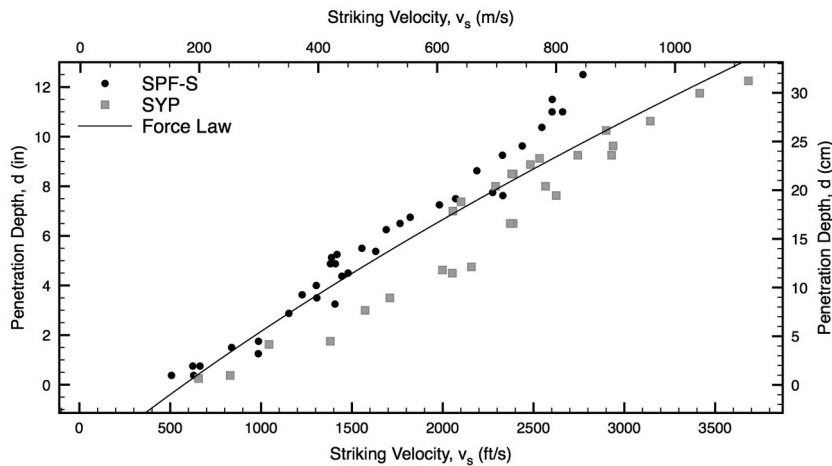


Fig. 12. Force Law penetration depth model calibrated with CLT data.

Table 6
Calibration constants for Force Law model for CLT.

| Data | Calibrated constants |
|-------------------|-----------------------------------|
| SPF-S and SYP CLT | $a = 3.550, b = 190.5, c = 574.7$ |

$$d = C_1 \left(\frac{v^a w^b}{\rho \left(\frac{\pi D^2}{4} \right)^c H^d} \right) \tag{12}$$

Using the experimental data and the procedures for calibrating constants discussed previously, the UFC equation for wood was re-calibrated for the CLT data to predict penetration depth. The results for both the SPF-S and SYP models as well as those from the original UFC equation are given in Fig. 14, with calibration constants given in Table 8. Note that the UFC calibration constants are those published in the UFC 4-023-07 and were not recalibrated to the data. The errors and comparison from the various models are discussed in the following section.

5.6. Model comparison and recommendations

Table 9 provides a summary of all the penetration depth models calibrated and/or developed in this research for CLT based on the two species of CLT considered. The table lists the model, constants, factors considered, and the mean square error (MSE) for the models.

The classical penetration mechanics models of Euler–Robins, Poncelet and Resal, along with the Force Law model, are all physics-based empirical models. The Force Law model, with a MSE of 1.32, was the best fitting model for the combined species CLT data set. The THOR models and the UFC model are curve-fitting empirical models. The THOR-based CLT model and the CLT UFC model performed better than the classical penetration models, likely because they include material parameters in the model. The THOR-based CLT model had a slightly better fit than the CLT UFC model. That said, all models that were recalibrated to the CLT data performed better than the existing model using the UFC equation for predicting the thickness of solid wood required to prevent perforation. This comparison is by now means all inclusive and additional models, such as those involving a linear approach [33–35] and those involving dimensionless optimization [36], could also be considered as a means to predict the response.

Based on this data set and the MSE, it is recommended that the THOR CLT model be used for predicting penetration depth for striking velocity ranging between 400 and 3,000 ft/s (120 to 910 m/s), for CLT of a thickness of greater than 4 in. (10.1 cm), and for projectiles with weights and areas similar to the 0.50 in. (12.7 mm) sphere projectile. Different weight, diameter, or nose shape projectiles could use a similar model, but it would require re-calibration of the model parameters. Additionally, for design purposes, a factor of safety should be implemented when determining how thick a CLT panel should be as there is variability in both the velocity of ballistic projectiles and in the wood material and it is expected that the CLT will provide less resistance near the back face. Further research is needed to quantify the effect of these these factors.

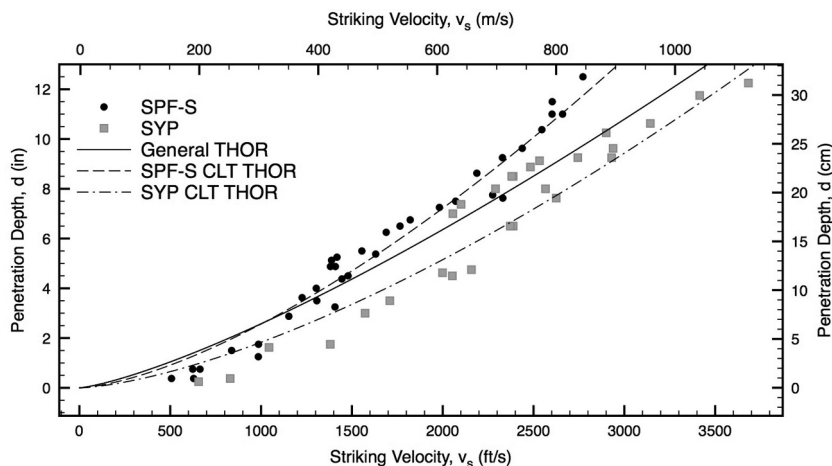


Fig. 13. General THOR model and CLT THOR model calibrated with CLT data.

Table 7
Calibration constants for general THOR and CLT THOR model.

| Model | Data | Calibrated constants |
|--------------|-------------------|---|
| General THOR | SPF-S and SYP CLT | $f = 1.305, g = 12.58, h = -3.967$ |
| CLT THOR | SPF-S and SYP CLT | $C_1 = 164.3, f = 1.493, g = 4.022, a = 1.373, b = 0.102$ |

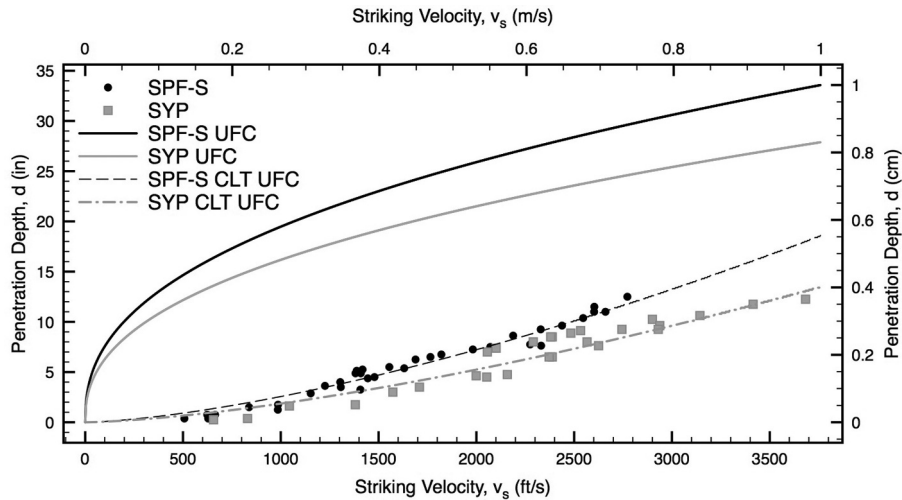


Fig. 14. UFC model and CLT UFC model calibrated with CLT data for both species of CLT.

Table 8
Calibration constants for CLT UFC model.

| Data | Calibrated constants |
|------------------|---|
| UFC Equation | $C_1 = 9, 837, a = 0.411, b = 1.490, c = 1.360, d = 0.541$ |
| CLT UFC Equation | $C_1 = 6.91e - 6, a = 1.495, b = 1.434, c = 0.201, d = 0.237$ |

It is important to note that while the curves developed with these models appear to continue on to predict more wood thickness required at high velocities, these models likely do not apply to the hypervelocity range. For this research, the velocity ranges evaluated are limited to the

intermediate velocity range, such as those seen with munitions projected from conventional weapons systems. Further evaluation would be needed for hypervelocity ranges, and it is likely that an upper bound exists for these models.

6. Residual velocity models

6.1. United facilities criteria (UFC) model

Similar to the equation for predicting the thickness of wood required to prevent perforation, the UFC 4-023-07 also has a suggested equation for predicting the residual velocity of a projectile that has

Table 9
Summary of models considered for predicting depth of penetration of CLT.

| Model | Equation | Constants | Parameters included | MSE |
|--------------|--|-------------------|--|-------|
| Euler–Robins | $d = \left(\frac{v_s^2}{2C_1} \right)$ | C_1 | striking velocity, v_s | 3.11 |
| Poncelet | $d = \frac{1}{2B} \ln \left(1 + \frac{Bv_s^2}{C} \right)$ | B, C | striking velocity, v_s | 1.34 |
| Resal | $d = \frac{1}{B} \ln \left(1 + \frac{Bv_s}{A} \right)$ | B, A | striking velocity, v_s | 1.71 |
| Force law | $d = \frac{1}{2a} (\sqrt{b^2 + 4v_s a - 4ac} - b)$ | a, b, c | striking velocity, v_s | 1.32 |
| General THOR | $d = \frac{1}{A} \left(\frac{v_s^f}{10^g w^h} \right)$ | f, g, h | striking velocity, v_s | 1.532 |
| CLT THOR | $d = C_1 \left(\frac{v_s^f}{10^g \rho^a H^b} \right)$ | C_1, f, g, a, b | projectile area, A projectile weight, w striking velocity, v_s | 0.303 |
| CLT UFC | $d = C_1 \left(\frac{v_s^f}{10^g \rho^a H^b} \right)$ | C_1, a, b, c, d | projectile weight, w target density, ρ target hardness, H striking velocity, v_s | 0.330 |
| | | | projectile weight, w projectile area, A target density, ρ target hardness, H | |

perforated through the wood [21]. This equation is given in Eq. (13), where v_r is the residual velocity, v_s is the striking velocity, T_w is the thickness required to prevent perforation, and t is the actual thickness of the wood.

$$v_r = v_s \left[1.0 - \left(\frac{t}{T_w} \right)^{0.5735} \right] \quad (13)$$

The 5-ply SPF-S (average thickness = 6.875 in (17.5 cm)) was used to demonstrate the fit of this equation. The CLT THOR model (Section 6.4) was used to estimate the value of T_w . Fig. 15 plots the experimental data for residual velocity, v_r . The plot also shows the line for the predicted residual velocity based on the suggested UFC equation. Additionally, the plot shows a newly calibrated model based on the generalized form given in Eq. (14), where the α is a calibration constant and d is the penetration depth determined by the CLT THOR model. In this case, the constant α was determined to be 1.643. This model is able to only acceptably predict the response over a small range of striking velocities centered around 2,500 ft/s (762 m/s).

$$v_r = v_s \left[1.0 - \left(\frac{t}{d} \right)^\alpha \right] \quad (14)$$

6.2. THOR-based residual velocity model

Because the calibrated THOR model was able to best predict the penetration depth (see Section 6.4 and Section 6.6), a new residual velocity model was developed to take advantage of this calibrated model, given in Eq. (11). The residual velocity, v_r , is zero when the final penetration depth, d , is exactly equal to (or less than) the thickness of the CLT, t . In other words, when the projectile stops exactly at the back face its residual velocity will be zero. If a new variable, v_{per} is defined as the perforation velocity or the maximum striking velocity that results in no perforation (i.e., residual velocity of zero), then Eq. (11) can be rewritten as in Eqs. (15) and (16).

$$v_s = \left(\frac{d}{C_1} (10^g \rho^a H^b) \right)^{(1/f)} \quad (15)$$

$$v_{per} = \left(\frac{t}{C_1} (10^g \rho^a H^b) \right)^{(1/f)} \quad (16)$$

The residual velocity, v_r , can then be computed as the difference between the striking velocity, v_s , and the perforation velocity, v_{per} . Because the projectile has less resistance near the back face of the CLT (see Fig. 5), it is expected that the residual velocities predicted by the equations derived in Section 6 will underpredict the actual residual

velocity. Because of this, a reduction factor, R , was added as a calibration factor. The resulting equation for residual velocity is therefore given in Eqs. (17) and (18).

$$v_r = v_s - R v_{per} \quad (17)$$

$$v_r = v_s - R \left(\frac{t}{C_1} (10^g \rho^a H^b) \right)^{(1/f)} \quad (18)$$

Eq. (18) calibrated with the 5-ply SPF-S data and a reduction factor, R , calibrated to 0.67 was determined to yield the minimum error. The curve associated with this new model is shown in Fig. 15 along with the results from the UFC residual velocity models. Clearly, this newly developed model does a better job at predicting the response than the other models, even those that were also calibrated to data. Because this data set consisted of only two wood species and one projectile, future research is recommended to validate this model over other ranges of parameters.

7. Conclusions

When investigating a new material, such as CLT, for ballistic penetration resistance, experimental testing is a critical first step. Testing helps build a database of parameters and responses that can be used to develop empirical models either through curve-fitting or applying physics-based methods. These models can in turn guide additional testing to further refine empirical models or analytical models. As the first set of ballistic experiments conducted on CLT, this research provides the critical first step. This research consisted of 152 ballistic experiments that were conducted at the U.S. Army Engineer Research and Development Center on two species of CLT: Spruce Pine Fir-South (SPF-S) and Southern Yellow Pine (SYP). Data was generated to understand and characterize the performance of the two species with varying thicknesses (i.e., number of plies in the CLT). In general, the SYP performed better, in terms of penetration resistance, than the SPF-S specimens. This is likely a function of the increased density and hardness of SYP relative to SPF-S. Experiments were also conducted to determine the effects of weathering (i.e., moisture content) on the ballistic performance. While the data set was limited, initial findings suggest that the effect of weathering on the ballistic performance within the ranges of velocity and moisture contents considered is negligible.

The CLT ballistic data sets were compared to current wood prediction models in the U.S. Unified Facilities Criteria. Results of this exercise showed the models do not accurately predict the embedment depth or residual velocity for CLT. A variety of models were developed and explored to better predict the responses, both classical (physics-based) and purely empirical. It was found that the models that

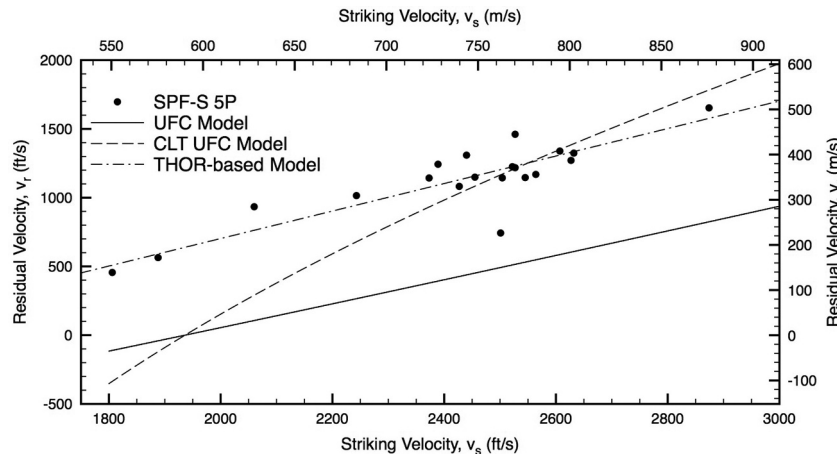


Fig. 15. 5 ply SPF-S residual velocity as a function of striking velocity with three predictive models: 1) UFC 4-023-07 wood model, 2) re-calibrated UFC model, and 3) calibrated THOR-based model.

incorporated the target material properties (i.e., CLT THOR or CLT UFC) were most accurate in predicting the penetration depth. An improved model that uses the CLT THOR model was developed and calibrated to predict the residual velocity in the cases of perforation. Most importantly, the results show the importance of correctly utilizing and re-calibrating existing models for new parameters (e.g., species, projectile type) that may be added in the future characterization the ballistic performance of CLT.

Acknowledgments

This work was supported by the United States Forest Service (USFS) through the Wood Innovations Grant under USFS Domestic Grant 17-DG-11083150-008. Any opinions, findings, and conclusions or recommendations expressed in this material are those of the authors and do not necessarily reflect the views of the United States Forest Service. The authors would like to acknowledge the support of Mr. Richard McGee, Mr. Don Little, Dr. Bill Heard, and Dr. Jesse Sherburn at the U.S. Engineer Research and Development Center and the support of Mr. Charles Rando and the U.S. Army Research Lab for their assistance with the experimental program.

References

- [1] Mohammad M., Gagnon S., Douglas B., Podesto L. Introduction to cross laminated timber. *Wood Design Focus*, 22(2).
- [2] Gagnon S, Pirvu C. *Cross laminated timber handbook*. SP-529E. FP Innovations; 2010.
- [3] Karacabeyli E, Douglas B. *CLT handbook u.s. edition*. 2013.
- [4] Levan S, Rowell R. *The chemistry of solid wood*. 207. American Chemical Society; 1984.
- [5] Ross R. *Wood handbook: wood as an engineering material*. centennial edition U.S. department of agriculture, forest products lab; 2010.
- [6] APA - The Engineered wood association, standard for performance-Rated cross-Laminated timber ANSI/APA PRG 320–2012. American National Standards Institute; 2012.
- [7] Brandner R, Flatscher G. *Cross laminated timber (clt): overview and development*. *Eur J Wood Wood Prod* 2016.
- [8] ASTM D905-08 - Standard test method for strength properties of adhesive bonds in shear by compression loading. American Society of Testing and Materials; 2013.
- [9] ASTM D5266-13 - standard practice for estimating the percentage of wood failure in adhesive bonded joints. American Society of Testing and Materials; 2013.
- [10] ASTM D143 - 94 Standard Test Methods for Small Clear Specimens of Timber. American Society of Testing and Materials; 2007.
- [11] Andrews C. *Wood in warfare*. 2012.
- [12] Meyer L, Brischke C, Welzbacher C. Dynamic and static hardness of wood: method development and comparative studies. *Int Wood Prod J* 2013;2:5–11.
- [13] Ceccotti A, Sandhass C, Okabe M, Yasumura M, Minowa C, Kawai N. Sofie project - 3d shaking table test on a seven-storey full-scale cross-laminated timber building. *Earthquake Eng Struct Dyn* 2013;42:2003–21.
- [14] Shiling P, van de Lindr J, Popovski M. Approximate r-factor for clt walls in multi-story buildings. *J Archit Eng* 2013;19(245–255).
- [15] Frangi A, Fontana M, Hugi E, Jubstl R. Experimental analysis of cross-laminated timber panels in fire. *Fire Saf J* 2009;44(8):1078–87.
- [16] CLT O. D.r. johnson passes two critical tests for safety of its cross-laminated timber panels – flame spread and fire resistance.
- [17] ASTM E84-15b - Standard method of test for burning characteristics of building materials. American Society of Testing and Materials; 2015.
- [18] ASTM E119-16 - Standard test methods for fire tests of building construction and materials. American Society of Testing and Materials; 2016.
- [19] Esler B. *Wood buildings survive second round of blast tests by usda and woodworks*. 2017.
- [20] Sanborn K. *Exploring cross-laminated timber use for temporary military construction: ballistic considerations*. Ph.D. thesis. Georgia Institute of Technology; 2018.
- [21] *Unified facilities criteria 4-023-07, design to resist direct fire weapons effects*. United States Department of Defense; 2008.
- [22] *UL 752 Ballistic standard*. 11 Underwriters Laboratory; 2005.
- [23] Rosenberg Z, Dekel E. *Terminal ballistics*. 2 Springer; 2016.
- [24] Warnis R. Using the poncelet penetration equation to predict the instantaneous velocity of a projectile in rice. *Tech. Rep. Air Force Armament Lan, Eglin AFB*; 1969.
- [25] Sparks J. *Basic terminal ballistics*.
- [26] Euler L. *The true principles of gunnery*. J Nourse; 1777.
- [27] Robins B. *New principles in gunnery*. 2 Wingrave; 1742.
- [28] Poncelet J-V. *Introduction a la mécanique industrielle*. 1938.
- [29] Resal C. C.r. 1895. p. 397–401.
- [30] More J. *The levenberg-marquardt algorithm: implementation and theory*. In: Watson G, editor. *Numerical Analysis. Lecture Notes in Mathematics*. 630. Springer; 1978.
- [31] Koene L, Broekhuis F. *Bullet penetration into wooden target*. 30th International Symposium on Ballistics. 2017.
- [32] Greenspon J. *An approximate nondimensional representation of the thor equations*. *Tech. Rep. US Army Mat System Anal Activity*; 1976.
- [33] Seisson G, et al. *Penetration and cratering experiments of graphite by 0.5-mm diameter steel spheres at various impact velocities*. *Int. J. Impact Eng.* 2014;70:14–20.
- [34] Heine A, Weber KE, Wickert M. *Experimental Investigation of the Penetration and Perforation of building materials by projectiles*. 26th International Symposium on Ballistics (12-16 Sept.). 2011.
- [35] Li Piani T, Koene L, Weerheijm J, Sluys LJ. *The Ballistic Resistance of Adobe Masonry: An analytical model for penetration in soil bricks and mortar*. *International Symposium on Ballistics Impacts on Structures (17th ISIEMS)*, Bad Neuenahr. 2017. p. 10–8.
- [36] Cunniff (1993) *paper entitled 'Dimensionless Parameters for Optimization of Textile Based Body Armor Systems*.